Chapter 1

Shell-Model Excited States and Collective Motion

"Experimentally, it is observed that nuclei can have several excited states... The nuclear shell model is instrumental in explaining these excited states."

lecture notes, PH5001

Ground-state I^π and Schmidt moments test the filling of the mean field. Excited states test whether the same orbitals, with particle promotions and pair breaking, organise the low-lying spectrum. Near closed shells the extreme shell model works well (classic example: ^{17}O). In mid-shell even–even nuclei the first 2^+ state is collective, and vibrational or rotational models are required [6, 1, 14].

1.1 Ground state of ^{17}O

Oxygen-17 has $Z = 8$, $N = 9$. Protons fill the closed shell through $1p_{1/2}$ (magic $Z = 8$) and contribute $I = 0$. Neutrons fill

$$(1s_{1/2})^2\,(1p_{3/2})^4\,(1p_{1/2})^2\,(1d_{5/2})^1. \tag{1.1}$$

The unpaired neutron is in $1d_{5/2}$ ($\ell = 2$, $j = \frac{5}{2}$), so

$$I^\pi = \tfrac{5}{2}^+, \tag{1.2}$$

matching experiment. The closed proton shell and nearly closed neutron p shell make ^{17}O a textbook single-particle nucleus: the core is ^{16}O and the valence neutron is weakly coupled to it.

1.2 Single-particle excitations of ^{17}O

Promoting the valence neutron to a higher empty orbit changes I^π without breaking the ^{16}O core:

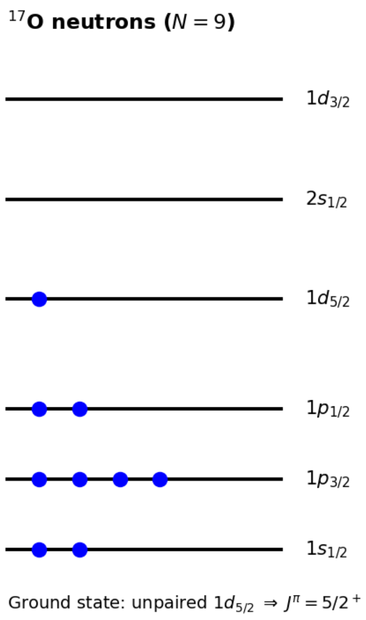

Figure 1.1: Neutron filling for ^{17}O. The ground state is fixed by the unpaired $1d_{5/2}$ neutron.

Configuration (valence n)	I^π	Character
$1d_{5/2}$	$\frac{5}{2}^+$	ground state
$2s_{1/2}$	$\frac{1}{2}^+$	first s-wave excitation
$1d_{3/2}$	$\frac{3}{2}^+$	spin–orbit partner of $d_{5/2}$

These positive-parity states appear in the low-lying spectrum and carry large single-particle strength in one-neutron transfer. Evaluated levels place the $1/2^+$ state at 871 keV and show additional positive- and negative-parity excitations consistent with sd and p-shell rearrangements [20, 21, 6].

1.3 Particle–hole excitations in ^{17}O

Higher states involve exciting a nucleon from a filled orbit, leaving a hole.

Hole in $1p_{3/2}$. Promote one neutron from $1p_{3/2}$ into $1d_{5/2}$. After the transition one has three neutrons in $1p_{3/2}$ (odd occupancy) and two in $1d_{5/2}$. The two $d_{5/2}$ particles can couple to $J_d = 0, 2, 4$, and this pair angular momentum must then couple to the $p_{3/2}$ hole:

$$I = |J_d - \tfrac{3}{2}|, \ldots, J_d + \tfrac{3}{2}, \qquad \pi = -. \tag{1.3}$$

Only the $J_d = 0$ component gives a pure $I^\pi = 3/2^-$ state; the full particle–hole configuration generates a negative-parity multiplet.

Hole in $1p_{1/2}$. Promote from $1p_{1/2}$ into $1d_{5/2}$: one unpaired neutron remains in $1p_{1/2}$. Coupling the $d^2_{5/2}$ pair $J_d = 0, 2, 4$ to the $p_{1/2}$ hole gives $I = |J_d - \frac{1}{2}|, \ldots, J_d + \frac{1}{2}$, all with negative parity. The $J_d = 0$ component gives $I^\pi = 1/2^-$, but it is not the only member.

Multi-particle couplings. When three unpaired neutrons sit in different orbits (e.g. $1p_{1/2}$, $1d_{5/2}$, $2s_{1/2}$), their angular momenta couple to several total I. Parity of a multi-particle configuration is the product of single-particle parities,

$$\pi = \prod_i (-1)^{\ell_i}. \tag{1.4}$$

A state such as $\frac{5}{2}^-$ can arise from coupling three unequal j values with overall negative parity. The extreme model still provides the language of orbits and parities even when residual interactions fix the detailed multiplet ordering.

1.4 Even–even example: ^{38}Ar

Argon-38 has $Z = 18$, $N = 20$. Neutrons fill the magic $N = 20$ shell; protons sit two holes below $Z = 20$. The ground state is even–even, so

$$I^\pi = 0^+. \tag{1.5}$$

Because $N = 20$ is closed, low-lying excitations often rearrange protons.

Proton $1d_{3/2} \to 1f_{7/2}$. In a restricted two-active-proton picture, paired spectator holes are assumed to carry $J = 0$. The remaining $d_{3/2}$ and $f_{7/2}$ angular momenta then run from $|7/2 - 3/2| = 2$ to $7/2 + 3/2 = 5$:

$$I = 2, 3, 4, 5, \qquad \pi = (-1)^2(-1)^3 = -. \tag{1.6}$$

States $2^-, 3^-, 4^-, 5^-$ are therefore allowed basis states. Residual interactions mix these with other cross-shell configurations and set their ordering; the triangle rule alone does not identify any evaluated level [6, 20, 21].

Proton $2s_{1/2} \to 1d_{3/2}$. With all other active particles paired to $J = 0$, the $s_{1/2}^{-1}d_{3/2}$ coupling allows $I^\pi = 1^+, 2^+$. This is a basis multiplet, not a prediction of its energy. Evaluated data instead provide the benchmark: ^{38}Ar has a first 2^+ level at 2167.6 keV, while a second 0^+ level occurs at 3377.5 keV and another 2^+ at about 3937 keV [20, 21]. Their wave functions require configuration mixing; none should be assigned from counting alone.

1.5 Systematics of the lowest 2^+ in even–even nuclei

In the great majority of even–even nuclei the lowest excited state is 2^+. Important exceptions occur near doubly closed shells, where a 0^+ or 3^- state may intervene; globally, however, a low-lying 2^+ cannot be explained by single-particle counting alone: the same pattern appears for hundreds of nuclei over a wide range of A (Fig. 1.2).

Empirical systematics of the lowest $E(2^+)$ show three regimes [6, 1, 14]:

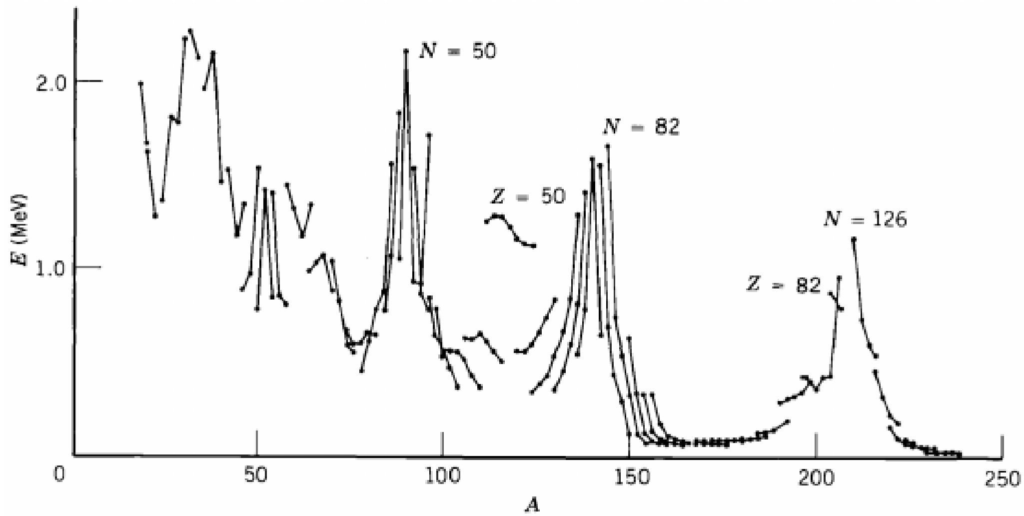

Figure 1.2: Energies of the lowest 2^+ states of even-Z, even-N nuclei versus A. Peaks occur at shell closures; mid-shell regions show much lower $E(2^+)$ (cf. Krane [6]).

1. **Magic and near-magic nuclei:** $E(2^+)$ is large (several MeV), reflecting rigid spherical cores.
2. **Spherical and weakly collective regions:** typical $E(2^+)$ values are of order 1 MeV. An approximately harmonic quadrupole vibrator has $E(4^+)/E(2^+) \approx 2$, while transitional nuclei need not obey this ideal ratio.
3. **Deformed regions $A \sim 150$–190 and $A \gtrsim 230$:** $E(2^+)$ drops to tens of keV, with $E(4^+)/E(2^+) \approx 10/3 \approx 3.33$, the rigid-rotor ratio.

Peaks of $E(2^+)$ at magic N or Z reconnect these collective trends to shell structure: closed shells stiffen the nucleus against deformation.

Key idea

Odd-A neighbours of closed shells: single-particle and particle–hole excitations. Even–even mid-shell nuclei: collective 2^+ (vibration or rotation). The shell model alone is incomplete for the latter.

1.6 Vibrational model

For spherical even–even nuclei ($A \lesssim 150$) the equilibrium shape is spherical. Small excess energy can excite volume-conserving surface oscillations. The nuclear radius is expanded in spherical harmonics,

$$R(\theta, \phi, t) = \bar{R}\left[1 + \sum_{\lambda=0}^{\infty} \sum_{\mu=-\lambda}^{\lambda} \alpha_{\lambda\mu}(t)\, Y_{\lambda\mu}(\theta, \phi)\right], \tag{1.7}$$

with multipolarity λ and deformation amplitudes $\alpha_{\lambda\mu}(t)$. Because R is real,

$$\alpha_{\lambda,-\mu} = (-1)^{\mu} \alpha^*_{\lambda\mu}. \tag{1.8}$$

Thus the $2\lambda+1$ complex-looking coefficients contain only $2\lambda+1$ independent real coordinates; quadrupole motion has five, not ten, real degrees of freedom. To derive the volume constraint, write the volume enclosed by the surface as

$$\mathcal{V} = \frac{1}{3}\int R^3(\theta,\phi,t)\,\mathrm{d}\Omega. \tag{1.9}$$

For small amplitudes, $(1+\epsilon)^3 = 1+3\epsilon+\mathcal{O}(\epsilon^2)$, so Eq. (1.7) gives

$$\begin{aligned}\mathcal{V} &= \frac{\bar{R}^3}{3}\int\left[1+3\sum_{\lambda\mu}\alpha_{\lambda\mu}Y_{\lambda\mu}\right]\mathrm{d}\Omega+\mathcal{O}(\alpha^2)\\ &= \frac{4\pi\bar{R}^3}{3}\left(1+\frac{3\alpha_{00}}{\sqrt{4\pi}}\right)+\mathcal{O}(\alpha^2),\end{aligned} \tag{1.10}$$

where $\int Y_{\lambda\mu}\mathrm{d}\Omega = \sqrt{4\pi}\,\delta_{\lambda 0}\delta_{\mu 0}$. Keeping $\mathcal{V} = 4\pi\bar{R}^3/3$ therefore requires

$$\alpha_{00} = 0 \qquad \text{to first order.} \tag{1.11}$$

At second order a small monopole correction compensates the volume change from $|\alpha_{\lambda\mu}|^2$. The intrinsic parity of a one-phonon excitation of multipolarity λ is $(-1)^\lambda$, because $Y_{\lambda\mu}(-\hat{r}) = (-1)^\lambda Y_{\lambda\mu}(\hat{r})$.

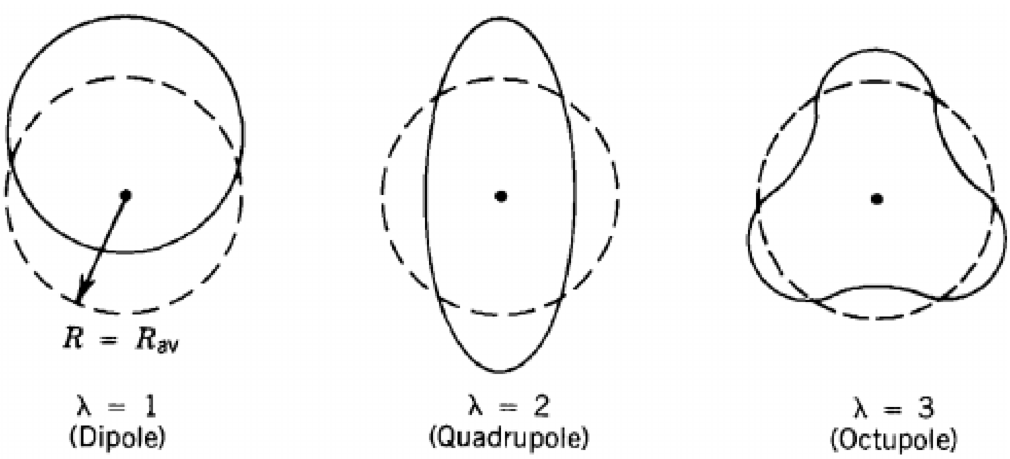

Figure 1.3: Lowest vibrational modes of a nucleus: dipole ($\lambda = 1$), quadrupole ($\lambda = 2$), octupole ($\lambda = 3$) (cf. Krane [6]).

Breathing mode ($\lambda = 0$). With $Y_{00} = 1/\sqrt{4\pi}$,

$$R(\theta,\phi,t) = \bar{R}\left(1+\frac{\alpha_{00}(t)}{\sqrt{4\pi}}\right). \tag{1.12}$$

The nucleus expands and contracts uniformly without changing shape. It is *not* an incompressible surface vibration: strict volume conservation sets the independent first-order α_{00} to zero. The physical isoscalar giant-monopole (breathing) resonance is a compressional density mode, lies at high excitation energy, and is outside the low-lying incompressible shape spectrum considered here.

Dipole mode ($\lambda = 1$). A pure $\lambda = 1$ surface deformation is equivalent to a displacement of the nuclear centre of mass. To see this explicitly, translate a sphere by a small vector $\boldsymbol{d}$. Along direction $\hat{r}$, its new surface is

$$R'(\hat{r}) = \bar{R} + \boldsymbol{d} \cdot \hat{r} + \mathcal{O}(d^2/\bar{R}). \tag{1.13}$$

The angular function $\boldsymbol{d} \cdot \hat{r}$ is a linear combination of the three $Y_{1\mu}$. Thus a $\lambda = 1$ deformation merely moves the whole sphere and can be removed by choosing the centre-of-mass origin. It is not an intrinsic excitation. Low-lying shape phonons begin at quadrupole order. (Giant dipole resonances are a different, high-energy isovector phenomenon in which protons and neutrons oscillate against each other.)

Quadrupole mode ($\lambda = 2$). The nucleus oscillates between prolate and oblate ellipsoidal shapes. This mode produces the dominant low-lying vibrational spectrum of spherical even–even nuclei.

Octupole mode ($\lambda = 3$). More complex pear-shaped surface oscillations; the one-phonon state is 3^-.

1.6.1 Phonons and the vibrational spectrum

After imposing the reality condition, each of the $2\lambda + 1$ independent real normal coordinates behaves as a harmonic oscillator. For one such coordinate the Hamiltonian has the form

$$H_{\lambda\mu} = \frac{\pi_{\lambda\mu}^2}{2B_\lambda} + \frac{1}{2} C_\lambda \alpha_{\lambda\mu}^2, \qquad \omega_\lambda = \sqrt{\frac{C_\lambda}{B_\lambda}}, \tag{1.14}$$

where B_λ is the collective inertia and C_λ the restoring-force constant. Canonical quantisation gives

$$E_{n_\lambda} = \left(n_\lambda + \tfrac{1}{2}\right) \hbar\omega_\lambda. \tag{1.15}$$

For a degenerate multipole there are $2\lambda + 1$ coordinates, so its vacuum zero-point energy is $(2\lambda + 1)\hbar\omega_\lambda/2$; for quadrupole motion it is $5\hbar\omega_2/2$, not $\hbar\omega_2/2$. Only excitation energies are relevant here, so that common offset is subtracted and n_λ phonons cost $n_\lambda\hbar\omega_\lambda$. These quanta are called **phonons**. The lowest vibrational excitation is one quadrupole phonon:

$$E = \hbar\omega_2, \qquad I^\pi = 2^+, \tag{1.16}$$

because the phonon carries angular momentum $\lambda = 2$ and parity $(-1)^\lambda = +$. For even–even nuclei the ground state is 0^+ and this 2^+ is the first excited state of the vibrational model.

Two quadrupole phonons have energy $2\hbar\omega_2$. Coupling two identical $I = 2$ bosons allows only the totally symmetric states $I = 0, 2, 4$ (the odd values $1, 3$ are forbidden for identical phonons), all with positive parity: the two-phonon triplet $0^+, 2^+, 4^+$.

Three quadrupole phonons give energy $3\hbar\omega_2$ and allowed $I^\pi = 0^+, 2^+, 3^+, 4^+, 6^+$. One octupole phonon gives

$$E = \hbar\omega_3, \qquad I^\pi = 3^-. \tag{1.17}$$

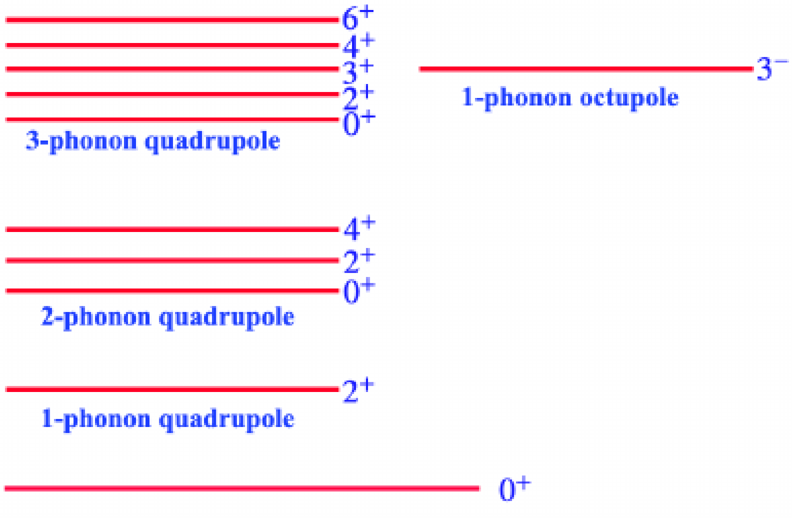

Figure 1.4: Schematic vibrational spectrum of an even–even nucleus: one-, two- and three-phonon quadrupole multiplets and the one-phonon octupole 3^-.

In the harmonic limit the two-phonon 4^+ and the one-phonon 2^+ satisfy

$$\frac{E(4^+)}{E(2^+)} = \frac{2\hbar\omega_2}{\hbar\omega_2} = 2, \tag{1.18}$$

matching the empirical ratio for many nuclei with $A \sim 30$–150. The equality is an ideal harmonic limit, not an exact universal rule: anharmonicities split the two-phonon multiplet and shift the ratio away from 2. For an incompressible liquid drop with surface tension σ and density ρ, the classical surface-mode frequencies scale as

$$\omega_\lambda = \sqrt{\frac{\sigma(\lambda-1)(\lambda+2)\lambda}{\rho\,\bar{R}^3}}, \tag{1.19}$$

so higher multipoles are stiffer and lie higher in energy [6, 1, 14].

1.7 Rotational model

Nuclei with large static quadrupole moments (notably $A \sim 150$–190 and $A \gtrsim 230$) are permanently deformed (Fig. 1.5). For an axially symmetric rotor the intrinsic deformation may be parametrised by a quadrupole parameter β_2 through

$$R(\theta) = \bar{R}(1 + \beta_2 Y_{20}(\theta) + \cdots). \tag{1.20}$$

Rotation about an axis perpendicular to the symmetry axis produces a quantized rotational band.

Classically $E = \frac{1}{2}\mathcal{I}\omega^2$ and $L = \mathcal{I}\omega$, so $E = L^2/(2\mathcal{I})$. In quantum mechanics the squared angular momentum of the rotor is replaced by $I(I+1)\hbar^2$, so

$$E_I = \frac{\hbar^2}{2\mathcal{I}}\,I(I+1). \tag{1.21}$$

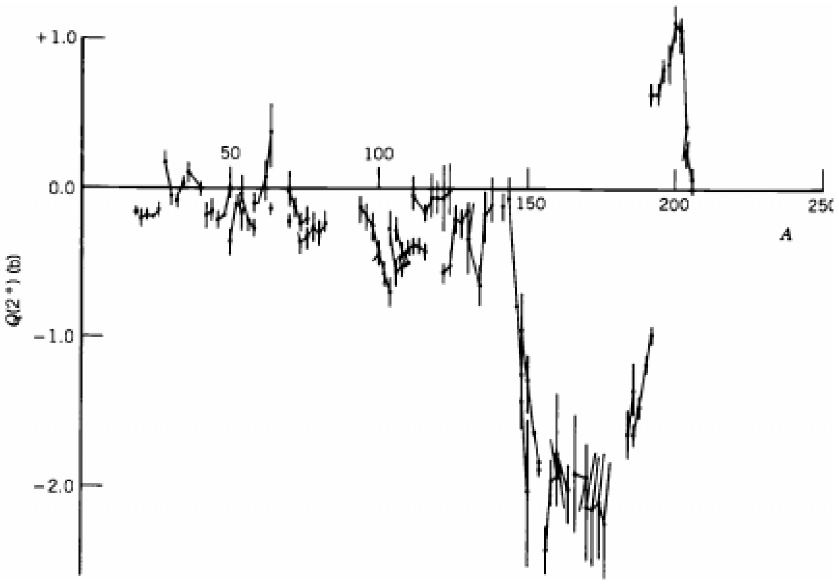

Figure 1.5: Electric quadrupole moments of the lowest 2^+ states of even–even nuclei. Large $|Q|$ in deformed regions signals permanent deformation (cf. Krane [6]).

For an axially symmetric intrinsic state, K is the projection of $\boldsymbol{I}$ on the symmetry axis. The sequence below assumes an even–even, reflection-symmetric ground configuration with $K = 0$, a single rigid moment of inertia, and invariance under a rotation by π about an axis perpendicular to the symmetry axis. Under these assumptions only even I with positive parity occur:

$$I^\pi = 0^+, 2^+, 4^+, 6^+, \ldots \tag{1.22}$$

(odd-I members are excluded). The first few energies are therefore

$$E(0^+) = 0, \tag{1.23}$$

$$E(2^+) = \frac{\hbar^2}{2\mathcal{I}}\, 2 \cdot 3 = \frac{6\hbar^2}{2\mathcal{I}}, \tag{1.24}$$

$$E(4^+) = \frac{\hbar^2}{2\mathcal{I}}\, 4 \cdot 5 = \frac{20\hbar^2}{2\mathcal{I}}, \tag{1.25}$$

and their ratio is

$$\frac{E(4^+)}{E(2^+)} = \frac{20}{6} = \frac{10}{3} \approx 3.33, \tag{1.26}$$

the classic rotor ratio. Rotational 2^+ energies are typically of order 10–100 keV, much lower than vibrational $\sim 1\,\mathrm{MeV}$ levels [6, 14, 1].

The same deformation that produces the rotational band also generates a large intrinsic quadrupole moment Q_0. For a uniformly charged, slightly deformed nucleus,

$$Q_0 \simeq \frac{3}{\sqrt{5\pi}}\, Ze\bar{R}^2\beta_2 \qquad \text{(to first order in } \beta_2\text{)}. \tag{1.27}$$

The laboratory spectroscopic quadrupole moment of a band member is

$$Q_s(I,K) = \frac{3K^2 - I(I+1)}{(I+1)(2I+3)}\,Q_0. \tag{1.28}$$

For the $K = 0$ ground-state band this is negative when $Q_0 > 0$: a prolate intrinsic shape does not imply a positive laboratory Q_s. The reduced transition probability is

$$B(E2; IK \to I-2, K) = \frac{5}{16\pi} Q_0^2 \,|\langle IK\,2\,0|I-2, K\rangle|^2\,. \tag{1.29}$$

Thus Q_s is linear in Q_0, whereas $B(E2)$ is quadratic in Q_0. Enhanced $B(E2)$ values (many Weisskopf units) are a hallmark of collective rotation, in contrast to single-particle estimates near closed shells [6, 1].

1.8 Limitations of the extreme shell model

The extreme single-particle picture fails when:

- several valence nucleons occupy an open shell (need configuration mixing and residual two-body matrix elements);
- the nucleus is soft or deformed far from magic numbers (collective rotational/vibrational degrees of freedom);
- continuum and cluster structures appear near drip lines.

Modern shell-model calculations keep the mean-field orbitals but diagonalise a residual interaction in a truncated valence space. Collective models build on the same single-particle structure: magic numbers still mark where sphericity is preferred.

Key idea

Near closed shells, excited states are particle promotions and particle–hole excitations on top of a magic core. ^{17}O is the cleanest example. Mid-shell even–even spectra demand collective vibration ($E(4^+)/E(2^+) \approx 2$) or rotation ($E(4^+)/E(2^+) \approx 3.33$).

1.9 Deeper physics: $E(2^+)$ systematics and collective ratios

1.9.1 Three regimes of the first 2^+ state

The lowest 2^+ excitation in even–even nuclei (Section 1.5) separates three physical regimes. Near doubly magic nuclei, $E(2^+) \sim 1$–$4\,$MeV: the core is spherical and particle–hole excitations cost shell-gap energy. In transitional nuclei, $E(2^+) \sim 0.5$–$1\,$MeV: quadrupole vibrations of a nearly spherical surface (Section 1.6) become competitive. In well-deformed rotors ($A \sim 150$–190, actinides), $E(2^+) \sim 10$–$100\,$keV: the entire nucleus rotates collectively (Section 1.7).

1.9.2 Vibration vs rotation: the energy ratio test

A harmonic quadrupole vibrator has equally spaced phonon levels, so

$$\frac{E(4^+)}{E(2^+)} \approx 2 \qquad \text{(vibrator)}, \tag{1.30}$$

while a rigid asymmetric rotor has

$$\frac{E(4^+)}{E(2^+)} = \frac{4(4+1) - 2(2+1)}{2(2+1) - 0(0+1)} = \frac{10}{3} \approx 3.33 \qquad \text{(rigid rotor)}. \tag{1.31}$$

These ratios are the quickest experimental discriminator between surface vibration and permanent deformation [6, 1].

^{152}Sm: a textbook rotor

^{152}Sm has $E(2^+) = 121.8\,\text{keV}$ and $E(4^+) = 366.5\,\text{keV}$, giving $E(4^+)/E(2^+) \approx 3.01$, close to $10/3$. The same nucleus in the samarium chain sits in the deformed rare-earth region where $B(E2; 0^+ \to 2^+)$ values are large (many collective nucleons). By contrast, ^{114}Cd near the $Z = 50$ shell shows $E(4^+)/E(2^+) \approx 2.0$–$2.4$, consistent with vibrational motion of a spherical core.

Remark

Shell-model incompleteness. The extreme single-particle model (Lecture 13) cannot produce hundreds of keV 2^+ states in mid-shell even–even nuclei: promoting one nucleon across a shell gap costs $\sim \hbar\omega \sim 10\,\text{MeV}$. Collectivity requires coherent motion of many nucleons. Peaks of $E(2^+)$ at magic N or Z (Figure 1.2) reconnect collective physics to the shell closures of Lecture 12.

1.9.3 $B(E2)$ as the dynamical partner of $E(2^+)$

The energy $E(2^+)$ locates the band head; the reduced transition probability $B(E2; 0^+ \to 2^+)$ measures collective quadrupole strength. Vibrators have moderate $B(E2)$; well-deformed rotors reach many Weisskopf units. A nucleus can have low $E(2^+)$ but small $B(E2)$ if the state is a two-phonon excitation rather than a rotor band head. Using energy ratios (1.30)–(1.31) together with $B(E2)$ disambiguates models that ratios alone leave degenerate [6, 14].

1.9.4 Phonons and the five quadrupole coordinates

The expansion (1.7) contains five independent real quadrupole amplitudes ($\lambda = 2$). Quantising these as harmonic oscillators gives a phonon spectrum with (1.30); rotors orient deformation in space and produce (1.31). The shell model of Lectures 12–14 supplies single-particle energies but not these collective coordinates, which is why vibration and rotation enter as complementary pictures [1, 6].

1.9.5 Critical-point analogy for shape transitions

The drop of $E(2^+)$ toward mid-shell even–even nuclei resembles a softening mode as the nucleus approaches a deformation instability. The ratio $E(4^+)/E(2^+)$ sliding from ~ 2 (vibrator) toward 10/3 (rotor) is an empirical order parameter for that transition. Microscopic theories (beyond-mean-field DFT, Monte Carlo shell model) aim to predict *where* on the chart the transition occurs without fitting $E(2^+)$ by hand. The shell closures of Lecture 12 mark the boundaries where the order parameter returns to large values (stiff spherical cores) [14, 43, 6].

Collective $B(E2)$ values can exceed Weisskopf units by orders of magnitude in rotors, while seniority-dominated near-spherical nuclei stay closer to single-particle estimates (Lecture 20). Shape coexistence in regions such as Ni or Hg isotopes shows low-lying 0^+ states whose charge radii and monopole strengths reveal deformed intruders. Use more than one observable before assigning a geometric label.

Ratio plus lifetime

Never assign a rotor on R_{42} alone; demand a lifetime or $B(E2)$. Conversely, a large $B(E2)$ with $R_{42} \sim 2.2$ may signal a transitional or coexistence regime rather than a textbook vibrator.

Physics-depth close

Collective models earn their keep when they predict ratios and trends, not when they decorate a single level energy with a geometric adjective. Demand $B(E2)$, monopole data, or radii before accepting a shape assignment.

1.10 Further physics: spectroscopic factors

One-nucleon transfer reactions such as (d, p) or (p, d) measure how much of a pure single-particle orbital is present in a nuclear state. The spectroscopic factor S quantifies that overlap: $S = 1$ for an ideal single-particle state on an inert closed core, while $S < 1$ signals fragmentation of the single-particle strength among several eigenstates [6, 1].

Near doubly magic cores, low-lying odd-A states often carry large spectroscopic factors, consistent with the extreme shell model. As one moves away from closed shells, residual interactions spread the strength and S decreases. Sum rules constrain the total strength available in a given orbit: the summed spectroscopic factors for adding or removing a nucleon from a closed shell cannot exceed the orbit's degeneracy. Fragmentation of spectroscopic strength is therefore direct experimental evidence for the limitations of the extreme independent-particle picture and for the need for configuration mixing or collective degrees of freedom.

1.10.1 Energy ratios as collective diagnostic

Collective models predict level spacing ratios that depend on the symmetry of the motion. For a harmonic quadrupole vibrator (Equation (1.30)),

$$E(0^+) = 0, \quad E(2^+) = \hbar\omega, \quad E(4^+) = 2\hbar\omega, \quad E(6^+) = 3\hbar\omega, \tag{1.32}$$

so $E(4^+)/E(2^+) = 2$ and $E(6^+)/E(2^+) = 3$. A rigid rotor (Equation (1.31)) gives $E(4^+)/E(2^+) = 10/3$ and $E(6^+)/E(2^+) = 7/3 \approx 2.33$. Transitional nuclei often fall between these limits, signalling γ-soft or shape-coexistence physics rather than pure vibration or rotation [6, 14].

1.10.2 Worked ratio: ^{152}Sm vs ^{114}Cd

^{152}Sm: $E(2^+) = 121.8\,\text{keV}$, $E(4^+) = 366.5\,\text{keV}$, ratio $= 3.01 \approx 10/3$ (rotor). ^{114}Cd: $E(2^+) \approx 558\,\text{keV}$, $E(4^+) \approx 1158\,\text{keV}$, ratio ≈ 2.08 (vibrator). The two nuclei sit on opposite sides of the $A \sim 150$ deformed region: Sm is mid-shell rare earth; Cd is near the $Z = 50$ shell closure where $E(2^+)$ rises (Figure 1.2) and collectivity weakens [6, 20].

1.10.3 Spectroscopic factors and the independent-particle limit

For (d, p) on ^{16}O populating the ^{17}O $d_{5/2}$ state, spectroscopic factors $S \approx 0.8$–1.0 confirm the extreme shell-model assignment (Lecture 13). In mid-shell nuclei, $S \sim 0.3$–0.5 is common: the same residual interactions that lower $E(2^+)$ fragment single-particle strength. Sum rules guarantee that total strength for a given orbit is conserved, but it spreads across many eigenstates [6, 1].

Single-particle vs collective $E(2^+)$ scale

Promoting one nucleon across a shell gap costs $\Delta\varepsilon \sim \hbar\omega \sim 10\,\text{MeV}$ (Lecture 12). Observed $E(2^+) \sim 100\,\text{keV}$ in deformed nuclei therefore requires $\sim 10^2$ nucleons contributing coherently to the quadrupole operator, not one valence nucleon. That 10^4 scale separation is the central reason collectivity lies outside the shell model of Lectures 12–14 [14].

1.10.4 Bridge to shell closures

Peaks in $E(2^+)$ at magic N or Z (Figure 1.2) mark where the shell model regains validity: closed shells resist deformation, so the first 2^+ is a particle–hole excitation, not a collective band head. The vibration/rotation ratio test is therefore most informative *between* magic numbers, where the filling diagram of Lecture 12 predicts mid-shell softness [1, 6].

1.10.5 Sum rule for spectroscopic strength

For a given single-particle orbit α, the sum of spectroscopic factors over all final states populated in one-nucleon transfer cannot exceed the degeneracy of α. When residual interactions spread strength, individual S values fall but the sum is preserved (up to reaction mechanism factors). Mid-shell nuclei with fragmented strength and low $E(2^+)$ therefore tell a consistent story: the independent-particle picture fails for *both* static moments (Lecture 14) and transfer strength at the same time [6, 1].

1.11 Deeper reading: $E(2^+)$, $B(E2)$, and shape coexistence

Vibrational nuclei have $E(4^+)/E(2^+) \simeq 2$; rigid rotors approach $10/3$. Real nuclei interpolate, and some exhibit shape coexistence: low-lying deformed and spherical configurations compete.

Monopole transition strengths and lifetime patterns distinguish scenarios that a single energy ratio cannot.

Large γ-ray arrays map these systematics across the chart, especially with radioactive beams. Microscopic theories aim to predict the onset of collectivity without fitted geometric parameters, connecting back to shell evolution (Lecture 12) and forward to isomer spectroscopy (Lecture 20). Plot $E(2^+)$ versus N for an isotopic chain as a standard student exercise: shell closures appear as peaks, deformation onsets as valleys.

Phase transitions in finite nuclei

The spherical–deformed transition can be discussed with control parameters such as valence nucleon number. Order parameters include β_2 deformation and $B(E2; 0^+ \to 2^+)$. Finite-system "phase transitions" are smoothed, yet energy-ratio trajectories still reveal rapid structural change. Pair that discussion with charge-radius kinks from Lecture 3.

Triaxiality

Rigid triaxial and soft γ-unstable models can yield similar low spin spectra. Higher spin levels, odd–even staggering of γ bands, and Coulomb excitation relative phases help discriminate. Do not assign triaxiality from a single $E(2^+)$ value.

Energy-ratio trajectory

For an isotopic chain (e.g. even–even Sm or Zr), plot $R_{42} = E(4^+)/E(2^+)$ versus N. Mark the vibrational locus near 2 and the rotational locus near 10/3. Identify where the chain crosses from one regime toward the other and whether a shape coexistence region is claimed in the literature. Add $B(E2)$ values if available: energies alone can mislead.

Connect to Lecture 3 by checking whether charge radii kink at the same neutron number where R_{42} drops. A simultaneous radius and collectivity change is strong evidence for deformation onset. Connect to Lecture 20 by asking how multipolarity assignments and lifetimes confirmed the 2^+ and 4^+ spin sequence used in the ratio.

Collectivity is organised by energy ratios, transition strengths, and radii together. No single observable deserves a geometric label on its own.

In practice, rework one numerical estimate from the lecture with a different parameter set and compare the shift to the quoted experimental uncertainty. If the shift exceeds the uncertainty, the estimate is teaching a scale, not delivering a fit. That distinction keeps theoretical cartoons honest when they sit beside evaluated data tables and modern many-body calculations. Along the course arc, write one sentence linking this chapter backward and one forward: the discipline of those two sentences is as important as any single formula. Examination problems rarely ask for a literature review, but they do ask for the scale argument that literature reviews presuppose.

Synthesis problem

Write a half-page note that (i) restates the chapter's central scale or selection rule in one equation, (ii) evaluates it numerically for one concrete nucleus or energy, and (iii) names the neighbouring lecture that uses the result. Keep the note free of research-frontier speculation; the goal is fluency with the lecture physics itself. If an assumption fails (Born approximation, spherical mean field, allowed transition, one-dimensional barrier), state the failure mode in a final sentence. That habit converts passive reading into examination-ready understanding and makes the later research-frontier box read as an extension rather than a replacement.

Research frontier: shapes, collectivity, and student projects

Vibrational and rotational models of Lecture 15 are the entry point to modern collective physics: shape coexistence, triaxiality, and quantum phase transitions between spherical, deformed, and γ-soft nuclei [43]. Large γ-ray tracking arrays and radioactive beams map $E(2^+)$, $B(E2)$, and monopole transition strengths across the chart, revealing where geometric models succeed and where microscopic configuration mixing is mandatory [51, 52]. Microscopic generators (beyond-mean-field density-functional theory, Monte Carlo shell model, and ab initio methods) aim to predict where collectivity onsets without fitted geometric parameters. Uncertainties that remain active research topics include the soft-γ versus rigid-triaxial distinction in transitional nuclei, the role of pairing in shape coexistence, and the quantitative accuracy of predicted $B(E2)$ values far from stability. The lecture's geometric language remains useful precisely when students learn its domain of validity.
For transitional nuclei, competing interpretations (shape coexistence versus a soft γ degree of freedom) can fit the same low-lying spectrum yet disagree on monopole strengths and lifetime patterns. Student projects that gather $E(0^+)$, $\rho^2(E0)$, and $B(E2)$ together learn how modern spectroscopy discriminates among collective scenarios.
Collecting $E(0^+)$, $\rho^2(E0)$, and lifetimes together is the modern way to test coexistence scenarios beyond a single $E(2^+)$ ratio.
Student directions. (1) Data project: from NuDat, plot $E(2^+)$ versus A for even-even Cd or Sm isotopes [21]. (2) Analytic check: compute the rigid-rotor ratio $E(4^+)/E(2^+)$ for one deformed nucleus and compare with 10/3. (3) Case study: identify one textbook case of shape coexistence and list the key experimental signatures.

1.12 Problems with solutions

Problem 15.1 — First excited state of ^{17}O

In the extreme single-particle model, what is I^π if the valence neutron of ^{17}O is promoted from $1d_{5/2}$ to $2s_{1/2}$? Compare with the evaluated excitation energy.

Solution 15.1

$2s_{1/2}$ has $\ell = 0$, $j = \frac{1}{2}$, so $I^\pi = \frac{1}{2}^+$. ENSDF places this state at 871 keV, matching the observed first excited state [20, 21, 6].

Problem 15.2 — ^{38}Ar multiplet

A proton is excited from $1d_{3/2}$ to $1f_{7/2}$ in ^{38}Ar. Assuming all spectator particles and holes couple to $J = 0$, list the allowed I^π values for the two active proton angular momenta. Explain why this does not determine the observed level ordering.

Solution 15.2

$j_1 = \frac{3}{2}$, $j_2 = \frac{7}{2}$ give

$$|j_1 - j_2| \le I \le j_1 + j_2 \quad \Rightarrow \quad I = 2, 3, 4, 5.$$

Parity $(-1)^{2+3} = -$, so $2^-, 3^-, 4^-, 5^-$ are allowed. Residual interactions and mixing with other cross-shell configurations determine their energies and strengths, so the triangle rule alone cannot assign an evaluated ^{38}Ar level [6, 20, 21].

Problem 15.5 — Extracting a rotor moment from $B(E2)$

For a $K = 0$ band,

$$B(E2; 2^+ \to 0^+) = \frac{Q_0^2}{16\pi}.$$

If $B(E2; 2^+ \to 0^+) = 0.50\, e^2\mathrm{b}^2$, find Q_0. Then give the spectroscopic moment $Q_s(2,0) = -2Q_0/7$.

Solution 15.5

$$Q_0 = \sqrt{16\pi B(E2)} = \sqrt{8\pi}\, e\mathrm{b} \approx 5.01\, e\mathrm{b}, \qquad Q_s(2,0) = -\frac{2}{7}Q_0 \approx -1.43\, e\mathrm{b}.$$

The negative laboratory Q_s is consistent with a positive intrinsic Q_0 for a prolate $K = 0$ rotor [6].

Problem 15.6 — Rotor prediction from one level

An even–even $K = 0$ band has $E(2^+) = 80\,\mathrm{keV}$. In the rigid-rotor limit, predict $E(4^+)$ and $E(6^+)$.

Solution 15.6

Since $E(I) = AI(I+1)$, $A = 80/6\,\mathrm{keV}$. Therefore

$$E(4^+) = \frac{20}{6}(80) = 267\,\mathrm{keV}, \qquad E(6^+) = \frac{42}{6}(80) = 560\,\mathrm{keV}.$$

Agreement with these ratios and enhanced in-band $B(E2)$ values are both needed before identifying a rotational band [6, 14].

Problem 15.3 — Rotor vs vibrator ratio

Compute $E(4^+)/E(2^+)$ for a pure axial rotor with $E(I) \propto I(I+1)$. Compare with the ideal harmonic vibrator value.

Solution 15.3

For the rotor,

$$E(2) \propto 2 \cdot 3 = 6, \qquad E(4) \propto 4 \cdot 5 = 20,$$

so the ratio is $20/6 = 10/3 \approx 3.33$. For a harmonic quadrupole vibrator, $E(4^+) = 2\hbar\omega_2$ while $E(2^+) = \hbar\omega_2$, so the ratio is 2 [6, 14].

Problem 15.4 — Why $\lambda = 1$ is not a shape phonon

Explain why a pure $\lambda = 1$ term in the surface expansion does not generate an intrinsic low-lying vibrational excitation.

Solution 15.4

A $\lambda = 1$ deformation displaces the nuclear surface in a way that is equivalent to a shift of the centre of mass. Transforming to the CM frame removes the amplitude, so there is no intrinsic shape excitation. Low-lying surface phonons therefore begin at quadrupole order ($\lambda = 2$) [6, 1].

Bibliography

[1] R. A. Dunlap, *An Introduction to the Physics of Nuclei and Particles* (2nd ed.), IOP Publishing, Bristol (2023), DOI: 10.1088/978-0-7503-6094-4, Ch. 3 (Nuclear composition and size).

[2] W. Demtröder, *Nuclear and Particle Physics*, Undergraduate Lecture Notes in Physics, Springer, Cham (2023).

[3] S. Petrera, *Problems and Solutions in Nuclear and Particle Physics*, UNITEXT for Physics, Springer, Cham (2019).

[4] F. Terranova, *A Modern Primer in Particle and Nuclear Physics*, Oxford University Press (2021).

[5] S. D'Auria, *Introduction to Nuclear and Particle Physics*, Undergraduate Lecture Notes in Physics, Springer, Cham (2018).

[6] K. S. Krane, *Introductory Nuclear Physics*, Wiley, New York (1988).

[7] R. Hofstadter, "Electron scattering and nuclear structure," Rev. Mod. Phys. **28**, 214 (1956).

[8] H. F. Ehrenberg, R. Hofstadter, U. Meyer-Berkhout, D. G. Ravenhall, and S. E. Sobottka, "High-Energy Electron Scattering and the Charge Distribution of Carbon-12 and Oxygen-16," Phys. Rev. **113**, 666 (1959).

[9] H. Yukawa, "On the interaction of elementary particles. I," Proc. Phys.-Math. Soc. Japan **17**, 48 (1935).

[10] R. D. Woods and D. S. Saxon, "Diffuse surface optical model for nucleon-nuclei scattering," Phys. Rev. **95**, 577 (1954).

[11] H. G. J. Moseley, "The high-frequency spectra of the elements," Phil. Mag. **26**, 1024 (1913); **27**, 703 (1914).

[12] C. F. von Weizsäcker, "Zur Theorie der Kernmassen," Z. Phys. **96**, 431 (1935).

[13] P. Cappellaro, *Introduction to Applied Nuclear Physics* (MIT OpenCourseWare / LibreTexts), CC BY-NC-SA 4.0.

[14] J.-L. Basdevant, J. Rich, and M. Spiro, *Fundamentals in Nuclear Physics: From Nuclear Structure to Cosmology*, Springer, New York (2005).

[15] D. Tong, *Particle Physics*, Lecture notes (University of Cambridge / CERN school notes).

[16] M. G. Mayer, "On closed shells in nuclei. II," Phys. Rev. **75**, 1969 (1949).

[17] O. Haxel, J. H. D. Jensen, and H. E. Suess, "On the "magic numbers" in nuclear structure," Phys. Rev. **75**, 1766 (1949).

[18] T. Schmidt, "Über die magnetischen Momente der Atomkerne," Z. Phys. **106**, 358 (1937).

[19] L. W. Nordheim, "On spins, moments, and shells in nuclei," Phys. Rev. **78**, 294 (1950).

[20] Evaluated Nuclear Structure Data File (ENSDF), National Nuclear Data Center, Brookhaven National Laboratory, `https://www.nndc.bnl.gov/ensdf/`.

[21] NuDat 3, National Nuclear Data Center, Brookhaven National Laboratory, `https://www.nndc.bnl.gov/nudat3/`.

[22] N. J. Stone, "Table of nuclear magnetic dipole and electric quadrupole moments," At. Data Nucl. Data Tables **90**, 75 (2005); updated compilations at NNDC.

[23] W. N. Cottingham and D. A. Greenwood, *An Introduction to Nuclear Physics* (2nd ed.), Cambridge University Press, Cambridge (2001).

[24] H. Geiger and J. M. Nuttall, "The ranges of the α particles from the radioactive substances," Phil. Mag. **22**, 613 (1911).

[25] G. Gamow, "Zur Quantentheorie des Atomkernes," Z. Phys. **51**, 204 (1928).

[26] R. W. Gurney and E. U. Condon, "Wave mechanics and radioactive disintegration," Nature **122**, 439 (1928); Phys. Rev. **33**, 127 (1929).

[27] M. Wang, W. J. Huang, F. G. Kondev, G. Audi, and S. Naimi, "The AME 2020 atomic mass evaluation (II). Tables, graphs and references," Chin. Phys. C **45**, 030003 (2021).

[28] Laboratoire National Henri Becquerel (LNHB), Recommended decay data, `http://www.lnhb.fr/nuclear-data/nuclear-data-table/`.

[29] L. M. Langer, R. D. Moffat, and H. C. Price, Jr., "Low energy beta-ray spectra: P^{32} and Cu^{64}," Phys. Rev. **76**, 1725 (1949).

[30] L. M. Langer and H. C. Price, Jr., "Shapes of the beta-spectra of the forbidden transitions of Sb^{124}, Rb^{86}, Sr^{89}, Y^{91}, and Cs^{137}," Phys. Rev. **75**, 1769 (1949).

[31] D. C. Camp and L. M. Langer, "The shape of the ^{66}Ga positron spectrum and the contribution from $0^+ \to 0^+$ transitions," Phys. Rev. **129**, 1782 (1963).

[32] H. C. Verma, *Nuclear Physics: Fundamentals and Applications*, NPTEL/IIT Kanpur lecture series, `https://hcverma.in/ncl_phy_lectures`.

[33] International Atomic Energy Agency, *LiveChart of Nuclides*, evaluated structure, decay, reaction, and fission-yield data, `https://www-nds.iaea.org/relnsd/vcharthtml/VChartHTML.html`.

[34] T. Kibédi, T. W. Burrows, M. B. Trzhaskovskaya, P. M. Davidson, and C. W. Nestor, Jr., "Evaluation of theoretical conversion coefficients using BrIcc," Nucl. Instrum. Methods Phys. Res. A **589**, 202 (2008), DOI: 10.1016/j.nima.2008.02.051.

[35] D. A. Brown *et al.*, "ENDF/B-VIII.0: The 8th major release of the nuclear reaction data library with CIELO-project cross sections, new standards and thermal scattering data," Nucl. Data Sheets **148**, 1 (2018), DOI: 10.1016/j.nds.2018.02.001.

[36] B. Acharya *et al.*, "Solar fusion III: New data and theory for hydrogen-burning stars," Rev. Mod. Phys. **97**, 035002 (2025), DOI: 10.1103/8lm7-gs18.

[37] S. N. Ghoshal, "An experimental verification of the theory of compound nucleus," Phys. Rev. **80**, 939 (1950), DOI: 10.1103/PhysRev.80.939.

[38] D. Adhikari *et al.* (PREX Collaboration), "Accurate determination of the neutron skin thickness of ^{208}Pb through parity-violation in electron scattering," Phys. Rev. Lett. **126**, 172502 (2021), DOI: 10.1103/PhysRevLett.126.172502.

[39] B. T. Reed, F. J. Fattoyev, C. J. Horowitz, and J. Piekarewicz, "Implications of PREX-II on the equation of state of neutron-rich matter," Phys. Rev. Lett. **126**, 172503 (2021), DOI: 10.1103/PhysRevLett.126.172503.

[40] B. Hu *et al.*, "Ab initio predictions link the neutron skin of ^{208}Pb to nuclear forces," Nature Phys. **18**, 1196 (2022), DOI: 10.1038/s41567-022-01715-8.

[41] E. Epelbaum, H.-W. Hammer, and U.-G. Meißner, "Modern theory of nuclear forces," Rev. Mod. Phys. **81**, 1773 (2009), DOI: 10.1103/RevModPhys.81.1773.

[42] H.-W. Hammer, S. König, and U. van Kolck, "Nuclear effective field theory: Status and perspectives," Rev. Mod. Phys. **92**, 025004 (2020), DOI: 10.1103/RevModPhys.92.025004.

[43] T. Otsuka, A. Gade, O. Sorlin, T. Suzuki, and Y. Utsuno, "Evolution of shell structure in exotic nuclei," Rev. Mod. Phys. **92**, 015002 (2020), DOI: 10.1103/RevModPhys.92.015002.

[44] H. Hergert, S. K. Bogner, T. D. Morris, A. Schwenk, and K. Tsukiyama, "The in-medium similarity renormalization group: A novel ab initio method for nuclei," Phys. Rep. **621**, 165 (2016), DOI: 10.1016/j.physrep.2015.12.007.

[45] J. M. Lattimer and M. Prakash, "The equation of state of hot, dense matter and neutron stars," Phys. Rep. **621**, 127 (2016), DOI: 10.1016/j.physrep.2015.12.005.

[46] J. M. Lattimer, "Neutron stars and the nuclear matter equation of state," Annu. Rev. Nucl. Part. Sci. **71**, 433 (2021), DOI: 10.1146/annurev-nucl-102419-124827.

[47] B. P. Abbott *et al.* (LIGO Scientific Collaboration and Virgo Collaboration), "GW170817: Observation of gravitational waves from a binary neutron star inspiral," Phys. Rev. Lett. **119**, 161101 (2017), DOI: 10.1103/PhysRevLett.119.161101.

[48] M. J. Dolinski, A. W. P. Poon, and W. Rodejohann, "Neutrinoless double-beta decay: Status and prospects," Annu. Rev. Nucl. Part. Sci. **69**, 219 (2019), DOI: 10.1146/annurev-nucl-101918-023407.

[49] M. Agostini, G. Benato, J. A. Detwiler, J. Menéndez, and F. Vissani, "Toward the discovery of matter creation with neutrinoless $\beta\beta$ decay," Rev. Mod. Phys. **95**, 025002 (2023), DOI: 10.1103/RevModPhys.95.025002.

[50] P. Gysbers *et al.*, "Discrepancy between experimental and theoretical β-decay rates resolved from first principles," Nature Phys. **15**, 428 (2019), DOI: 10.1038/s41567-019-0450-7.

[51] H. L. Crawford, K. Fossez, S. König, and A. Spyrou, "A vision for the science of rare isotopes," Annu. Rev. Nucl. Part. Sci. **74**, 141 (2024), DOI: 10.1146/annurev-nucl-121423-091501.

[52] Nuclear Science Advisory Committee, *A New Era of Discovery: The 2023 Long Range Plan for Nuclear Science*, U.S. Department of Energy and National Science Foundation (2023), `https://nuclearsciencefuture.org/`.

[53] S. A. Giuliani, Z. Matheson, W. Nazarewicz, E. Olsen, P.-G. Reinhard, J. Sadhukhan, B. Schuetrumpf, N. Schunck, and P. Schwerdtfeger, "Colloquium: Superheavy elements: Oganesson and beyond," Rev. Mod. Phys. **91**, 011001 (2019), DOI: 10.1103/RevModPhys.91.011001.

[54] N. Schunck and D. Regnier, "Theory of nuclear fission," Prog. Part. Nucl. Phys. **125**, 103963 (2022), DOI: 10.1016/j.ppnp.2022.103963.

[55] I. Counts, J. Hur, D. P. L. Aude Craik, H. Jeon, C. Leung, J. C. Berengut, A. Geddes, A. Kawasaki, W. Jhe, and V. Vuletić, "Evidence for nonlinear isotope shift in Yb^+ search for new boson," Phys. Rev. Lett. **125**, 123002 (2020), DOI: 10.1103/PhysRevLett.125.123002.

[56] I. Angeli and K. P. Marinova, "Table of experimental nuclear ground state charge radii: An update," At. Data Nucl. Data Tables **99**, 69 (2013), DOI: 10.1016/j.adt.2011.12.006.

[57] S. Kraemer *et al.*, "Observation of the radiative decay of the ^{229}Th nuclear clock isomer," Nature **617**, 706 (2023), DOI: 10.1038/s41586-023-05894-z.